Geophysical Prospecting, 2003, **51**, 61–74

Effects of an anisotropic overburden on azimuthal amplitude analysis in horizontal transverse isotropic media

Sonja Maultzsch,[1]* Steve Horne,[2] Stewart Archer[2] and Hans Burkhardt[3]

[1]*British Geological Survey, Murchison House, West Mains Road, Edinburgh EH9 3LA, UK,* [2]*WesternGeco, Schlumberger House, Buckingham Gate, Gatwick, West Sussex RH6 0NZ, UK, and* [3]*Fachgebiet Angewandte Geophysik, Technische Universität Berlin, Ackerstrasse 71–76, 13355 Berlin, Germany*

Received January 2002, revision accepted August 2002

ABSTRACT

Azimuthal amplitude variation in fractured media, commonly used to characterize fracture systems, is a function not only of reflection at the target but also of transmission through the overburden. This study investigates the sensitivity of amplitudes to various anisotropic overburden effects in horizontal transverse isotropic (HTI) media. Issues considered here are geometric spreading, transmission coefficients and attenuation due to fluid flow. Their influence on the azimuthal amplitude variation is evaluated quantitatively over a wide model space.

Only the variation of transmission coefficients with azimuth proves to be negligible. Geometric spreading alters the amplitude signature significantly over a relatively narrow range of models, and its influence increases with layer thickness. The most severe effect of an anisotropic fractured overburden is attenuation due to fluid flow between the cracks or the cracks and pores in the surrounding matrix. The relative changes in amplitudes between the symmetry directions due to anisotropic absorption are of the same order of magnitude as the changes in the reflection coefficient. The effect is significant over a very wide range of petrophysical parameters. Thus it leads to considerable problems in the amplitude analysis for almost any case of an overburden that contains cracks and pores. A correct amplitude analysis at the target will not be possible unless the effect of attenuation is removed.

INTRODUCTION

Azimuthal elastic anisotropy observed in the earth is often caused by naturally occurring fracture systems. For a detailed characterization of underground reservoirs and predictions of possible fluid pathways, it is of great interest to gain information about the orientation of fractures, their size and the nature of crack infill, from geophysical data. Seismic velocities and amplitudes are often used for that purpose. For their analysis the rock is generally assumed to contain vertically aligned cracks, so that it can be represented as a homogeneous horizontal transverse isotropic (HTI) medium in the long wavelength limit.

There exist various approximate representations of the reflection coefficient in HTI media (e.g. Mallick, Chambers and Gonzalez 1996; Rüger 1996; Kühnel 1998) that form the basis of the amplitude analysis (often called AVOAz analysis). The function of reflected amplitudes is symmetric about certain azimuths that coincide with the orientations of the symmetry planes in the anisotropic material (i.e. the fracture strike and the fracture normal). The magnitude of the azimuthal amplitude variation is used to estimate structural crack parameters. For a long time, studies were focused on these reflectivity aspects, and the interpretation of amplitudes was based only on signatures of the plane-wave reflection

*E-mail: smau@bgs.ac.uk. Formerly at [2] and [3].

coefficient (e.g. Rüger and Tsvankin 1997; Pérez, Gibson and Toksöz 1999; Gray and Head 2000). On the other hand, it has been found in many real data cases that the results of the amplitude analysis differ substantially from the results of the velocity analysis. These discrepancies may be caused by transmission through an anisotropic overburden. In this case, the transmission coefficients, geometric spreading and attenuation also contribute to the azimuthal changes in amplitudes that are observed in the data.

Horne and MacBeth (1997) investigated transmission effects in connection with VSP data and concluded that transmission coefficients can be neglected but attenuation might be an issue. MacBeth *et al*. (1997) and Kühnel (1998) found that they needed to calibrate the amplitudes prior to the AVOAz analysis with a reflection just above the target to eliminate overburden effects and obtain correct results. Mallick *et al*. (1998) either neglected the effect of geometric spreading or applied a spreading correction using a v^2t-expression as in isotropic media but as a function of the anisotropic NMO velocity field. This is, however, not correct in the anisotropic case and ray tracing has to be performed instead to evaluate the correct divergence factors.

Hudson, Liu and Crampin (1996) and Pointer, Liu and Hudson (2000) have given theories describing anisotropic attenuation due to fluid flow in cracked porous rock as a function of structural parameters, fluid properties and frequency. They proposed three different mechanisms of pressure-releasing flow that dissipate elastic energy. Pointer *et al*. (2000) discussed the frequency dependence of each mechanism in great detail. Concerning seismic frequencies, the question remains: how does the amount of attenuation vary with fluid and crack properties and over which parameter ranges does it alter the amplitude signature significantly? MacBeth (1999) showed the effect of anisotropic attenuation on seismic amplitudes in a modelling study. However, the suggested relaxation time seems to be too high for realistic geological parameter values.

In general, there is a need for quantitative investigations into the effects of an anisotropic overburden when considering a general model space. In fact, these issues were often neglected without knowledge of their contribution to the observed azimuthal amplitude variation.

We performed seismic modelling in order to quantify the influence of the three overburden effects (geometric spreading, transmission coefficients and attenuation) on the change of amplitude with azimuth. In comparison with the azimuthal variation of reflection coefficients, we can determine whether they present a serious problem for azimuthal amplitude analysis, leading to erroneous results unless they are removed.

EFFECTIVE MEDIUM THEORY

The modelling of the elastic coefficients that represent the fractured rock as an equivalent homogeneous anisotropic medium followed Hudson's theory (Hudson 1981, 1986). The cracks are assumed to be penny-shaped, i.e. they have the form of oblate spheroids. The theory expresses the effective stiffness tensor $\mathbf{c}$, accurate to second order in crack density ε, as

$$\mathbf{c} = \mathbf{c}^{(0)} + \varepsilon\mathbf{c}^{(1)} + \varepsilon^2\mathbf{c}^{(2)}, \tag{1}$$

where $\mathbf{c}^{(0)}$ is the isotropic stiffness tensor of the background medium, $\mathbf{c}^{(1)}$ are the first-order perturbations describing single scattering, and $\mathbf{c}^{(2)}$ accounts for crack–crack interaction. For HTI media containing vertical cracks with the crack normals aligned along the x-axis, $\mathbf{c}^{(1)}$ can be written as follows:

$$\mathbf{c}^{(1)} = -\frac{1}{\mu}\begin{pmatrix} (\lambda+2\mu)^2U_{11} & \lambda(\lambda+2\mu)U_{11} & \lambda(\lambda+2\mu)U_{11} & 0 & 0 & 0 \\ \lambda(\lambda+2\mu)U_{11} & \lambda^2U_{11} & \lambda^2U_{11} & 0 & 0 & 0 \\ \lambda(\lambda+2\mu)U_{11} & \lambda^2U_{11} & \lambda^2U_{11} & 0 & 0 & 0 \\ 0 & 0 & 0 & 0 & 0 & 0 \\ 0 & 0 & 0 & 0 & \mu^2U_{33} & 0 \\ 0 & 0 & 0 & 0 & 0 & \mu^2U_{33} \end{pmatrix} \tag{2}$$

with

$$U_{11} = \frac{4}{3}\left(\frac{\lambda+2\mu}{\lambda+\mu}\right)/(1+K), \tag{3}$$

where

$$K = \frac{a}{\pi c}\frac{\kappa_f + 4/3\mu_f}{\mu}\left(\frac{\lambda+2\mu}{\lambda+\mu}\right),$$

and

$$U_{33} = \frac{16}{3}\left(\frac{\lambda+2\mu}{3\lambda+4\mu}\right)/(1+M), \tag{4}$$

where

$$M = \frac{4a}{\pi c}\frac{\mu_f}{\mu}\left(\frac{\lambda+2\mu}{3\lambda+4\mu}\right).$$

U_{11} and U_{33} are the responses of the crack to normal and shear traction, respectively. λ and μ are the Lamé parameters of the background rock, and κ_f and μ_f are the bulk modulus and the shear modulus of the crack content. The aspect ratio of the cracks, i.e. the semi-minor axis divided by the semi-major axis, is denoted by c/a. The second-order contribution $\mathbf{c}^{(2)}$ is given in terms of $\mathbf{c}^{(1)}$ as (Hudson 1986):

$$c^{(2)}_{ijkl} = \frac{1}{\mu} c^{(1)}_{ijrs}\, \chi_{rstu}\, c^{(1)}_{tukl}, \tag{5}$$

where

$$\chi_{rstu} = \left\{\delta_{rt}\delta_{su}\left(4 + v_S^2/v_P^2\right) - \left(\delta_{rs}\delta_{tu} + \delta_{ru}\delta_{st}\right)\left(1 - v_S^2/v_P^2\right)\right\}/15.$$

v_S and v_P are the S- and P-wave velocities of the host rock and δ_{ij} is the Kronecker delta. Extensions of these formulae to incorporate fluid flow and attenuation will be shown below. First we restrict ourselves to the case of isolated cracks where pressure equalization within the pore space does not take place.

Equivalently to Hudson's theory, the stiffness of the HTI medium can be expressed in terms of normal and tangential fracture compliances Z_N and Z_T. This formulation was used in Schoenberg's linear slip model (Schoenberg 1983; Schoenberg and Douma 1988), which is another effective medium theory. It describes the compliance tensor $\mathbf{s} = \mathbf{c}^{-1}$ as the sum of the background compliance $\mathbf{s}_b$ and the fracture compliance $\mathbf{s}_f$. For HTI symmetry, $\mathbf{s}_f$ contains only two independent elements, Z_N and Z_T. Hsu and Schoenberg (1993) introduced fracture weaknesses as dimensionless parameters that are related to Z_N and Z_T as follows:

$$\Delta_N = \frac{(\lambda + 2\mu)Z_N}{1 + (\lambda + 2\mu)Z_N} \text{ and } \Delta_T = \frac{\mu Z_T}{1 + \mu Z_T}; \quad 0 < \Delta_N < 1,\ 0 < \Delta_T < 1. \tag{6}$$

Since these parameters vary only between 0 and 1, they are very useful to describe a general model space, as required in parts of this study. Furthermore, they can always be related to structural parameters in other effective medium theories (Liu, Hudson and Pointer 2000). Comparison with Hudson's (1981) first-order theory shows that both Δ_N and Δ_T are proportional to the crack density. If the cracks are gas- or fluid-filled (zero shear modulus), Δ_T is unaffected by the type of infill. By contrast, Δ_N depends predominantly on the magnitude of the term $(\kappa_f/\mu)(a/c)$. In the case of isolated fluid-filled cracks with a small aspect ratio, this quantity tends to be very much greater than 1 and Δ_N tends to zero.

The plane-wave reflection coefficient at the boundary of an HTI medium varies with angle of incidence and azimuth. As an example, Fig. 1 shows the reflectivity signature for one of the models investigated in this study. The reflection originates from the base of an HTI layer containing brine-filled cracks with an aspect ratio of 0.001 and a crack density of 0.1. The crack normals are aligned with the x-axis, and the shotpoint is located at the origin. The parameters of the background model and the fluid properties are given in Tables 1 and 3. The plot demonstrates that azimuthal amplitude variation due to the reflection coefficient, which is large enough to be detected in the data, occurs at high offsets or angles of incidence (roughly between 30° and 40°). The need for these high angles of incidence in AVOAz analysis has also

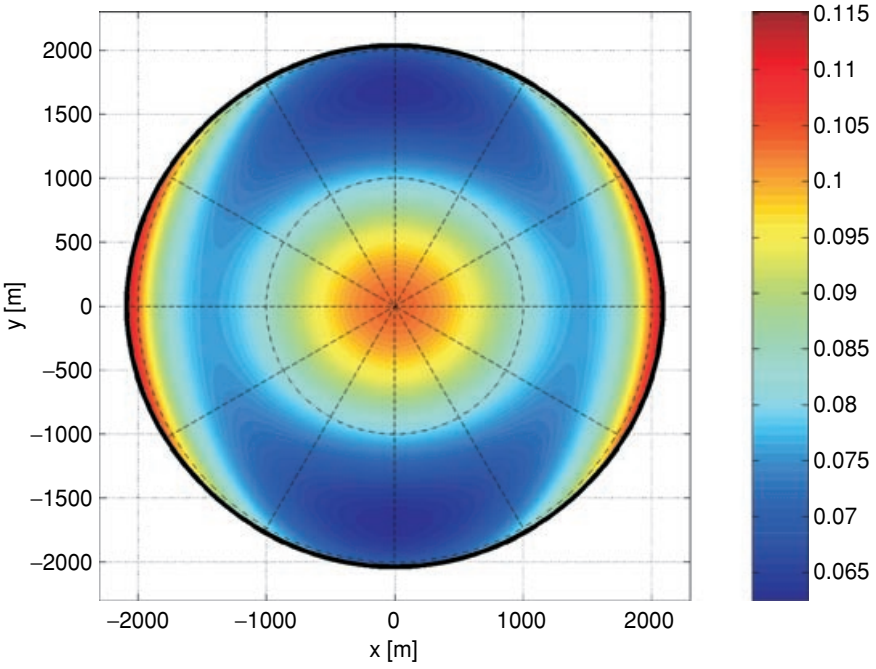

Figure 1 Plane-wave reflection coefficient at the base of an HTI layer, projected on to the surface (plane of acquisition). Crack faces are normal to the x-axis. The crack density is 0.1, the aspect ratio is 0.001 and the cracks are brine-filled. Significant azimuthal amplitude variation occurs at offsets above 1300 m or angles of incidence above 30°.

Table 1 Medium properties of the background model, that was used throughout the study

Layer	v_P (m/s)	v_S (m/s)	Density (kg/m^3)	Thickness (m)
(1) Isotropic	3400	1700	2400	1000
(2) HTI	4000	2400	2550	300
(3) Isotropic	4600	2760	2700	Half-space

Table 2 Anisotropy ranges for two v_S/v_P-ratios that were used in the computation of spreading factors

v_S/v_P	Δ_N	Δ_T
0.6	0–0.6	0–0.3
0.35	0–1.0	0–0.2

Table 3 Properties of the different types of crack infill

Fluid	v_P (m/s)	Density (kg/m^3)	Viscosity (Pa.s)
Gas	620	65	0.00002
Brine	1710	1100	0.001
Oil	1250	800	0.02

been reported in case studies (e.g. MacBeth *et al*. 1997; Lynn *et al*. 1999). Furthermore, they are used in the analysis of multi-azimuth walkaway VSPs (e.g. Horne *et al*. 1998), for which the results of this study are equally applicable. Therefore, we shall investigate the influence of overburden effects in this range of angles of incidence. Azimuthal amplitude analysis aims to recover the signature of the plane-wave reflection coefficient in order to deduce the orientation of the symmetry planes and crack properties.

GEOMETRIC SPREADING

Geometric spreading is defined as the loss of intensity along a portion of a wavefront bounded by a cone of rays. It can be evaluated from the ratio of the area spanned by the rays at the receiver to the corresponding area at the source. In anisotropic media, the raypaths are complicated functions of both direction-dependent group and phase velocities. Therefore the divergence effect is also direction-dependent and cannot be described in a simple way.

We performed extensive ray tracing on a range of models with one HTI layer embedded in two isotropic formations. The base of the HTI layer was taken as the target reflector. Model parameters are given in Tables 1 and 2. The values of the fracture weaknesses Δ_N and Δ_T were chosen to define the most general model space for the different v_S/v_P-ratios and, at the same time, to correspond to reasonable microstructural crack parameters according to Hudson's model. At crack densities much higher than 0.1, Hudson's theory becomes invalid. This was used as a limit for the model space. At the lower v_S/v_P-ratio, the S-wave velocity in the background model was decreased. It should be noted that the models with a v_S/v_P-ratio of 0.6 represent a more realistic case, since fractures are more likely to occur in harder rocks. The computations were performed for two thicknesses of the fractured layer: 300 m (as shown in Table 1) and 500 m, while the base of the layer was held at a constant depth of 1300 m. Spreading factors were calculated along 2D lines at azimuthal increments of 2.5°. The out-of-plane component appeared to be negligible, so that there was no need to perform the computations in 3D.

For a v_S/v_P-ratio of 0.6 and a 300 m-thick HTI layer, Fig. 2 shows the relative change in divergence factors between the fracture strike and the fracture normal, defined by $[\mathrm{div}(90^\circ) - \mathrm{div}(0^\circ)]/\mathrm{div}(0^\circ)$, over the entire model space. The quantity was evaluated at a constant incident phase angle of 40°. From the plot, we can read directly how much the amplitudes change between the symmetry directions due to the spreading effect alone and compare it to the change in the reflection coefficient at that particular angle of incidence. Figure 3 presents the results of the same computations but for a 500 m-thick HTI layer. As mentioned above, high angles of incidence were chosen for all calculations, where the azimuthal variation in reflected amplitudes is generally significant enough to be analysed accurately.

The figures demonstrate that the largest anisotropic effect of the geometric spreading occurs at high values of Δ_T and low values of Δ_N. In terms of Hudson's microcrack model this corresponds to isolated fluid-filled cracks with a high crack density. The maximum values of the plotted relative amplitude change lie around 10% for a 300 m-thick layer and increase up to 15% at a layer thickness of 500 m. For the major part of the model space, however, the geometric spreading causes amplitude variations below 10% between the fracture strike and the fracture normal. Since the changes in reflectivity that we are trying to analyse are clearly above 10% (see Fig. 1), only cases with fluid-filled cracks, high crack densities and a very thick fractured layer could be problematic for the amplitude analysis, if the spreading effect is not corrected for in an appropriate way.

Figures 4 and 5 display the corresponding results for a v_S/v_P-ratio of 0.35 for a 300 m and a 500 m-thick HTI layer, respectively. Here the incident phase angle is 30°. The signatures of these plots are different from those found above

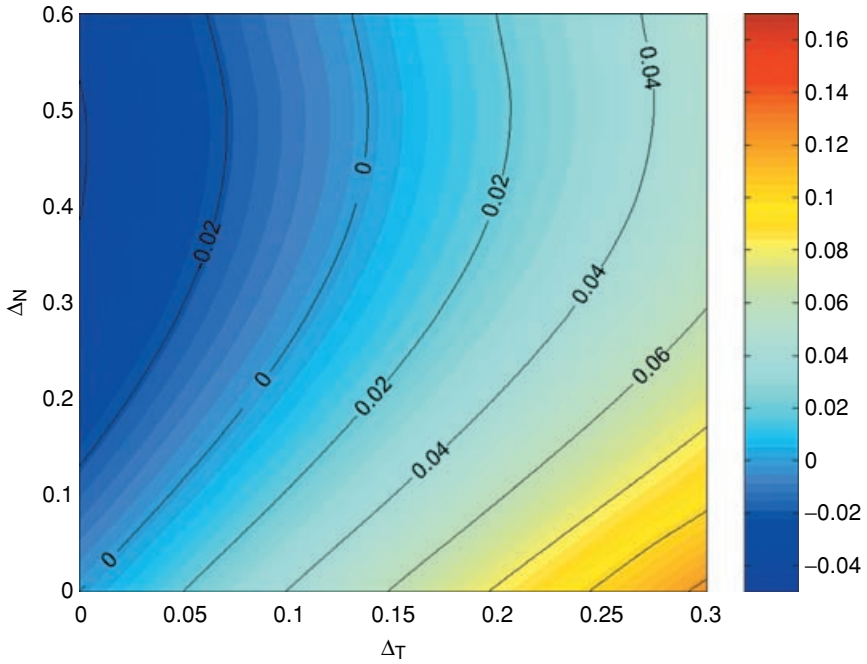

Figure 2 Relative change in divergence factors between the fracture strike and the fracture normal, [div(90°) − div(0°)]/div(0°), as a function of fracture weaknesses Δ_N and Δ_T at an incident phase angle of 40°. $v_S/v_P = 0.6$, thickness of HTI layer = 300 m. The quantity is positive for most of the model space, i.e. divergence factors increase towards the fracture normal. The maximum values occur for fluid-filled cracks with a high crack density (= low Δ_N, high Δ_T) and lie around 10%.

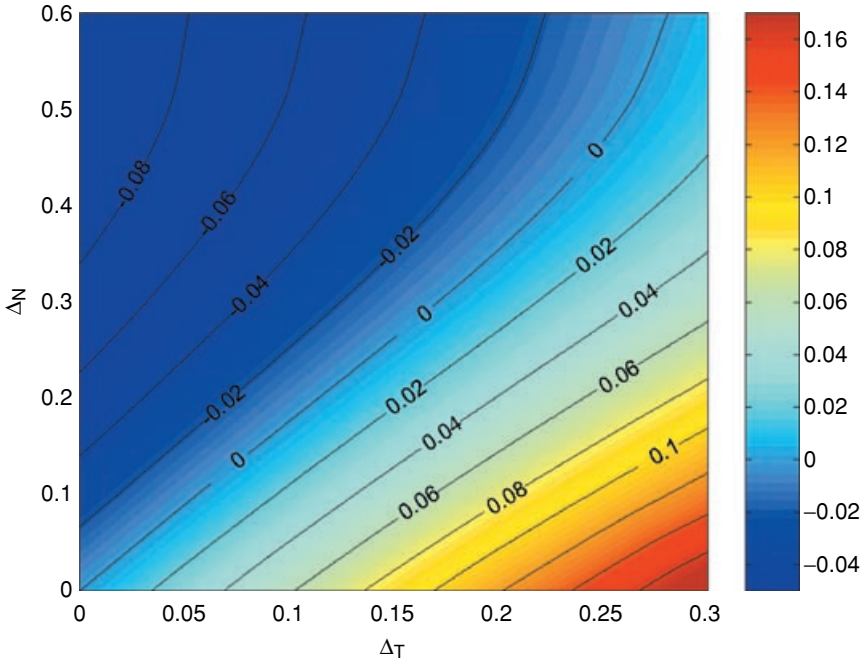

Figure 3 As Fig. 2 for a layer thickness of 500 m. Values of the azimuthal change in divergence factors are increased; maxima are around 15%.

(Figs 2 and 3). Now the maxima occur at high values of Δ_N and increase slightly with Δ_T. Translated into Hudson's model, this corresponds to gas-filled cracks with high crack porosity, i.e. a high crack density and aspect ratio. Again the maximum relative amplitude change that the geometric spreading may produce lies between 10% and 15% and comprises only a small part of the model space.

Overall, the results demonstrate that there are cases where the divergence effect yields significant azimuthal amplitude variations that also have to be considered in the amplitude

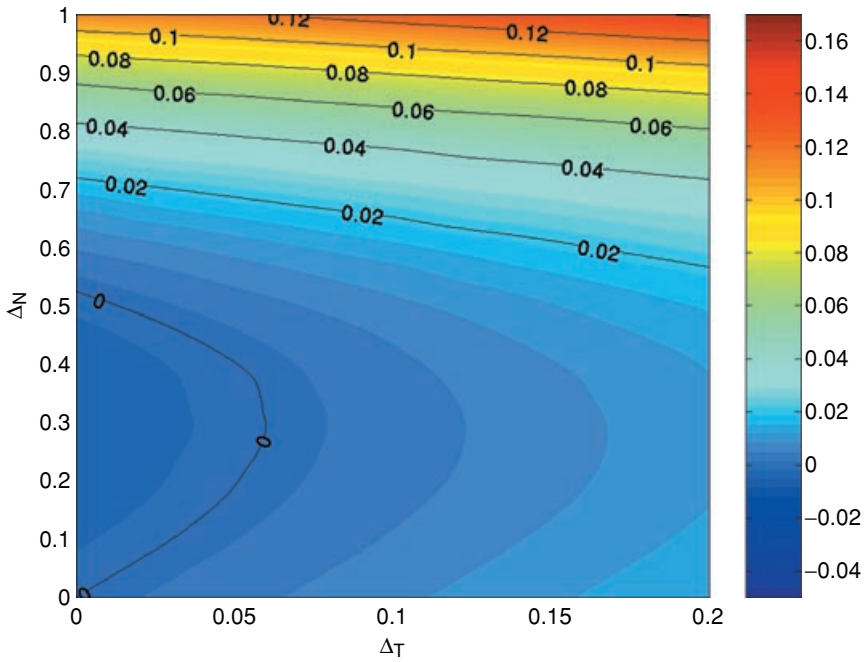

Figure 4 Relative change in divergence factors between the symmetry directions for $v_S/v_P = 0.35$ and a layer thickness of 300 m at an incident phase angle of 30°. The maximum values occur for high Δ_N and increase with Δ_T (= gas-filled cracks with a high crack porosity).

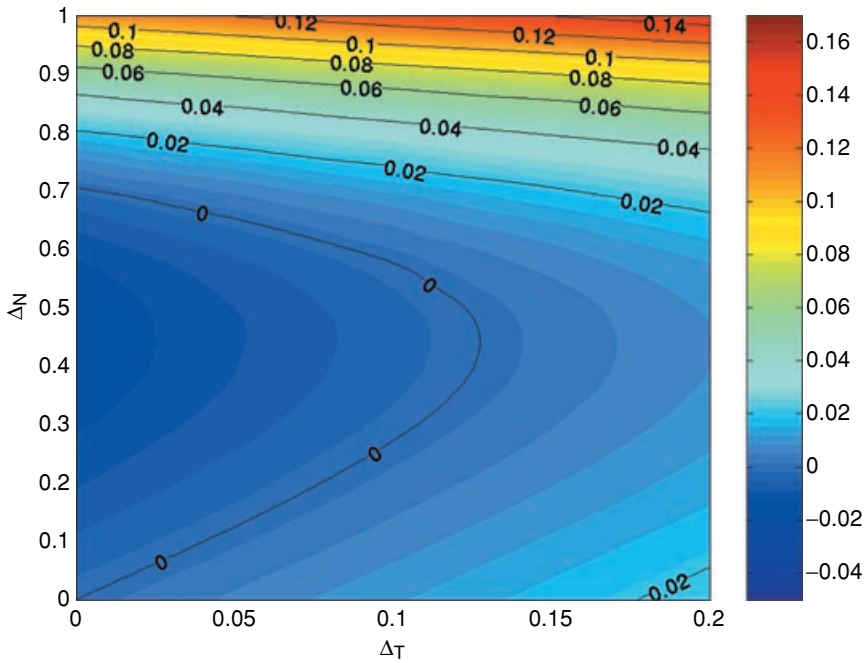

Figure 5 As Fig. 4 for a layer thickness of 500 m. The maximum values are slightly increased.

analysis. How these cases are defined depends on the v_S/v_P-ratio of the host rock. In general, the anisotropic behaviour of the geometric spreading increases with layer thickness. It should also be kept in mind that this is only one of the overburden effects, and it adds to the transmission coefficients and attenuation. For many models, however, the results suggest the use of the velocity function of the fracture strike for an isotropic geometric spreading correction. The errors in amplitudes introduced by this procedure will be within acceptable limits.

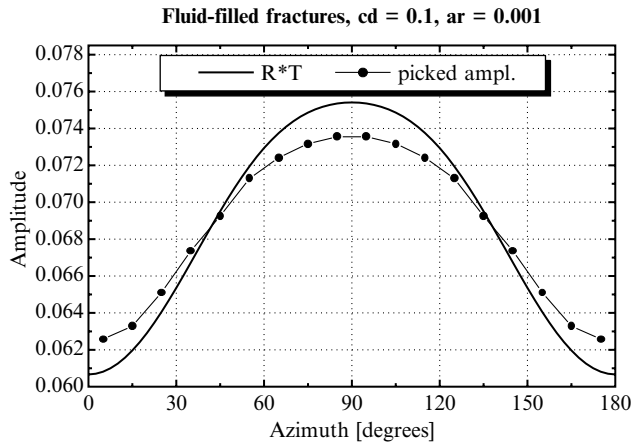

Figure 6 Synthetic data example to demonstrate the effect of the geometric spreading on azimuthal amplitude variation. The model contains brine-filled cracks with a crack density of 0.1 and an aspect ratio of 0.001. The remaining model parameters are given in Tables 1 and 3. The dots are the amplitudes picked from the data at an incident phase angle of 35°. The solid line is the reflection coefficient at the base of the HTI layer multiplied by the transmission coefficients at the top of that layer. Changes in amplitudes between the symmetry directions due to the spreading effect are relatively small.

Figure 6 shows the effect in a synthetic data example. The model used here has brine-filled cracks with an aspect ratio of 0.001 and a crack density of 0.1. The remaining model parameters are given in Tables 1 and 3. Corresponding values of Δ_N and Δ_T are 0.005 and 0.23, respectively. The figure shows the amplitudes, picked from the data at an incident phase angle of 35°, plotted against azimuth. The azimuth in this and all subsequent figures is always measured from the fracture strike. For comparison, the curve of the reflection coefficient multiplied by the transmission coefficients of the upcoming and the downgoing wavefield is shown. There is no attenuation in the cracked layer, so that the differences seen in the two curves are due to the spreading effect only. The resulting errors are relatively small and the symmetry directions can still be found correctly. Only the estimation of crack parameters might be slightly incorrect.

A method was proposed by Mallick *et al.* (1998) to correct for the geometric spreading by using a v^2t-expression as in isotropic materials and the anisotropic NMO velocity field. Since this function scales the amplitudes to different values at zero offset, it was suggested that they should be normalized to the same intercept again after the correction had been applied. The results of this study, however, demonstrate that a v^2t-type correction with NMO velocities will introduce even more errors than treating the model as isotropic. The plots in Figs 2 and 3 indicate, for instance, that the anisotropy of divergence factors at a high v_S/v_P-ratio is larger for fluid-than for gas-filled cracks. Gas-filled cracks, on the other hand, exhibit a stronger anisotropy in NMO velocities.

The approach of defining the divergence factor in terms of NMO velocities, derived by Newman (1973), is valid only for isotropic homogeneous layered media. The derivation assumes rotational symmetry about the vertical axis through the shotpoint, and a connection between the geometry of raypaths is made through the phase velocities. In anisotropic materials, however, the raypath geometry can be defined only through the direction-dependent group and phase velocity field, which basically requires knowledge of all independent stiffness components. The rotational symmetry is not given either, so that spreading factors cannot be derived in a straightforward way.

TRANSMISSION COEFFICIENTS

The same background model as above (see Table 1) and a range of crack parameters was used to compute transmission coefficients at the top of the HTI layer for both the downgoing and the upcoming wavefield. The azimuthal variation of the transmission coefficients appeared to be very small over the entire model space. The relative amplitude change between the symmetry directions does not exceed 2%. Maximum values occur for fluid-filled cracks with high crack porosity. A corresponding example is shown in Fig. 7, where the crack faces are again normal to the x-axis. Since the amplitude variation produced by the transmission coefficients is not likely to be above the noise level in a real data case, they can be neglected in the amplitude analysis. Only in the very unusual case of a set of multiple fractured layers, where the fractures have the same orientation in each layer, could the transmission coefficients become an issue.

If we compare Fig. 7 to Fig. 2, we see that for the same model the transmission coefficients yield a slight increase in amplitudes normal to the fractures, whilst the spreading effect produces a decrease in that direction. This holds for the majority of the model space, so that these two overburden effects cancel each other out to some degree.

ATTENUATION

Hudson's theory has been extended to include three different mechanisms of attenuation due to fluid flow (Hudson *et al.* 1996; Pointer *et al.* 2000). These are the only currently available theories that allow the modelling of anisotropic

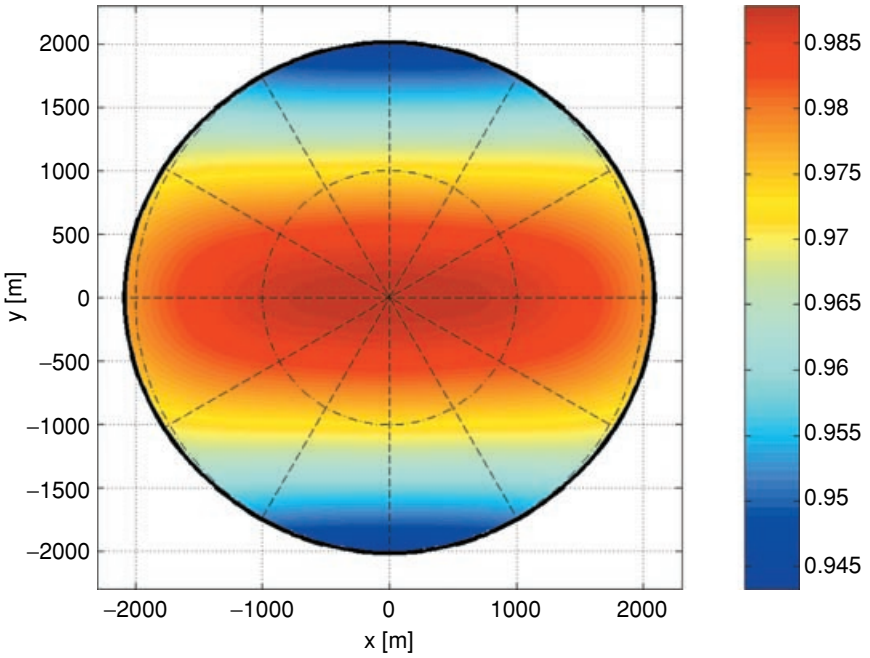

Figure 7 Transmission coefficients at the top of the HTI layer for a model with brine-filled cracks, a crack density of 0.1 and an aspect ratio of 0.001. The azimuthal variation is very small and maximum amplitude changes between the symmetry directions are 2%. (An offset of 2000 m corresponds to an angle of incidence of approximately 43°.)

attenuation coefficients or quality factors as functions of petrophysical parameters and frequency. The three mechanisms are relaxation processes caused by fluid flow. They occur:

1 within isolated cracks that are partially saturated;
2 between interconnected cracks via microscopic pathways;
3 between cracks and pores in the surrounding matrix (equant porosity).

They are easily incorporated into Hudson's (1981) model by modifying the expressions for U_{11} and U_{33} in (3) and (4). Since the number of variables is increased (parameters such as permeability, porosity and fluid viscosity have to be considered as well), there is no simple way to quantify the effect of anisotropic attenuation for a general model space. Therefore only the dependence on a few key parameters will be demonstrated. The frequency in all the calculations was held constant at 30 Hz.

Partially saturated cracks

If cracks are partially saturated with liquid and partially with gas, the different compressibilities of the two materials have the effect that, under pressure, fluid is driven into spaces previously occupied by gas. The magnitude of attenuation depends strongly on the compressibility contrast of the two infill materials. We have found that in all cases of two-phase fluids that can be expected in reservoirs, these magnitudes are very small at seismic frequencies, so that the effect on the amplitude signature can be neglected. Therefore partially saturated cracks will not be discussed further in this paper. Nevertheless it should be noted that the mechanism has to be taken into account if data in other frequency ranges, such as borehole data, are considered.

Interconnected cracks

To account for fluids moving between cracks interconnected by microscopic pathways, the quantities K and M in (3) and (4) need to be modified to (Hudson *et al.* 1996; Pointer *et al.* 2000):

$$K = \left\{\frac{a}{\pi c}\frac{\kappa_f}{\mu}\left(\frac{\lambda+2\mu}{\lambda+\mu}\right)\right\}\left\{1-\frac{3\mathrm{i}\,\kappa_f\,k^2\,K_r a}{4\pi\varepsilon\omega\eta_f c}\right\}^{-1}; \tag{7}$$

$$M = \frac{4a}{\pi c}\frac{\mathrm{i}\omega\eta_f}{\mu}\left(\frac{\lambda+2\mu}{3\lambda+4\mu}\right), \tag{8}$$

where K_r denotes the overall permeability of the rock, η_f denotes the fluid viscosity, k denotes wavenumber and ω denotes angular frequency. K now includes the effect of pressure release through fluid flow, while the change in M accounts for the viscosity of the crack content. The variables of interest, on which the amount of attenuation depends, are the permeability, the fluid viscosity and the aspect ratio.

Figures 8 and 9 show plots of the imaginary part of U_{11} versus permeability for different aspect ratios and viscosities. The quantity $\mathrm{Im}(U_{11})$ can be taken as a qualitative measure of the amount of P-wave attenuation, since the real part of the stiffness coefficients is governed by the background stiffness values.

The plots show that for thin cracks, attenuation increases with increasing permeability and decreasing viscosity (note the difference in the vertical scale of the plots). It was mentioned by Pointer *et al.* (2000) that diffusion for the interconnected crack model does not occur locally, but has to be effective over a wavelength scale. For seismic frequencies the time for pressure equalization to take place is relatively long, but also the distances between pressure maxima and minima are large. Therefore, it is physically plausible that at those frequencies a high diffusivity allows the pressure to equalize more effectively, which leads to an increase in attenuation. At the left end of the permeability scale in Figs 8 and 9, the cracks approach the state of being isolated and fluid- or gas-filled, so that there is no attenuation. If the permeability is increased above 1 D and the viscosity is further decreased, the cracks will be essentially drained and act as if they were empty. Attenuation would tend to zero as well at this state. However, realistic parameter ranges are those shown in the figures.

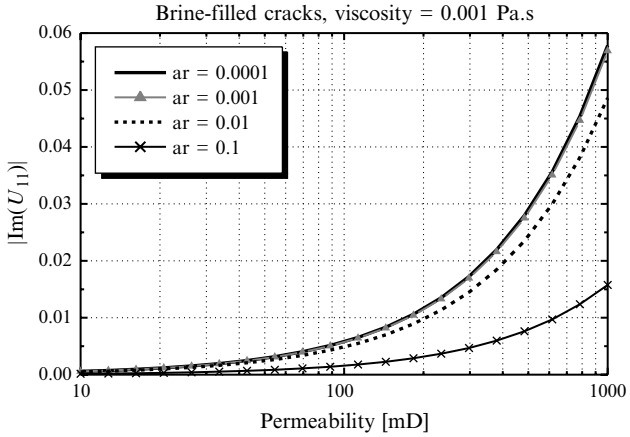

Figure 8 Dependence of the imaginary part of U_{11} on permeability and aspect ratio for interconnected cracks at a frequency of 30 Hz. Cracks are brine-filled. Values increase with permeability and decrease with aspect ratio.

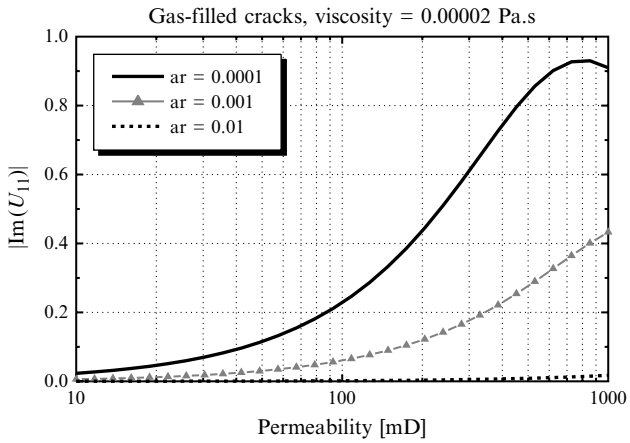

Figure 9 As Fig. 8 for a model with gas-filled cracks. Values are increased (compare vertical scales of Figs 8 and 9) and a maximum is reached at an aspect ratio of 0.0001 and high permeabilities.

Attenuation also increases with decreasing aspect ratio, which is less intuitive. From (7) we can see that lowering the aspect ratio has the same effect as increasing the fluid bulk modulus or the crack-space compressibility, and thus the magnitude of attenuation rises. Since this phenomenon is not dependent on the particular mechanism of pressure releasing flow, it is applicable to the other two attenuation models as well.

In order to demonstrate what the above plots mean in terms of attenuated amplitudes, attenuation coefficients and amplitudes were computed over a large model space, defined by the background model from Table 1, with gas fill, an aspect ratio of 0.0001, crack densities of 0.01 and 0.1, and permeability values ranging from 50 mD to 1 D. In the same way as the quantity evaluated for the geometric spreading (Figs 2–5), the relative change in amplitudes between the fracture strike and the fracture normal due to attenuation, $[\mathrm{A}(90^\circ) - \mathrm{A}(0^\circ)]/\mathrm{A}(0^\circ)$, was computed at an incident phase angle of 40°.

Figure 10 shows a plot of this quantity as a function of permeability for two values of crack density. As expected, the amount of attenuation perpendicular to the fractures increases with permeability and at high permeability values it is significantly larger for a higher crack density. Over a range of permeabilities from 500 mD to 1 D and at a crack density of 0.1, the amplitudes change by 11% to 21% between the symmetry directions, due to attenuation. These magnitudes are already comparable to the amount of azimuthal variation in reflection coefficients that we try to extract from the data. Even if the crack density is decreased by a factor of 10 to a value of 0.01, the relative amplitude change reaches 11% at the high permeability end. Thus, attenuation due to fluid flow between interconnected cracks considerably alters the signature of reflected amplitudes over a fairly wide range of parameters.

To demonstrate the effect in a data example, synthetic seismograms were generated for a model with gas-filled cracks, an aspect ratio of 0.0001, a crack density of 0.1 and a permeability of 1 D. A zero-phase wavelet with an amplitude spectrum centred around 30 Hz was used. Figure 11 shows the amplitudes picked from the data as a function of azimuth at an incident (phase) angle of 40° in comparison with the reflection coefficient (solid line). We find that in this case the decrease in amplitudes perpendicular to the fractures, which is caused by the reflectivity, is more than doubled due to attenuation. Although the symmetry directions can still be found from the data, the correct estimation of crack parameters will not be possible. Instead the data would suggest a model with entirely different properties.

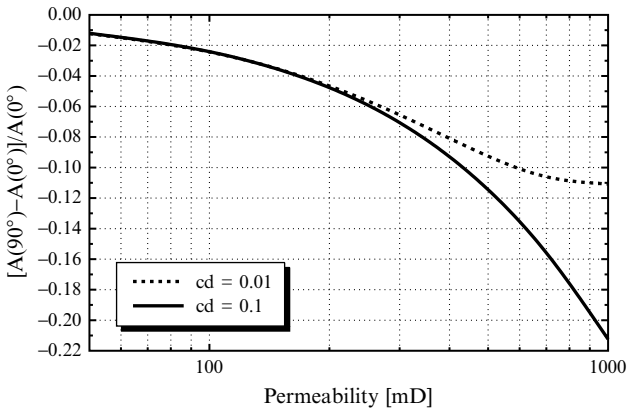

Figure 10 Interconnected cracks, relative change in attenuated amplitudes between the symmetry directions, $[A(90^\circ) - A(0^\circ)]/A(0^\circ)$, for gas fill and an aspect ratio of 10^{-4}. Variation with permeability and crack density. Amplitudes were computed at an incident phase angle of 40°. The azimuthal amplitude variation is significant for permeabilities from 500 mD to 1 D and it increases strongly with crack density over that range.

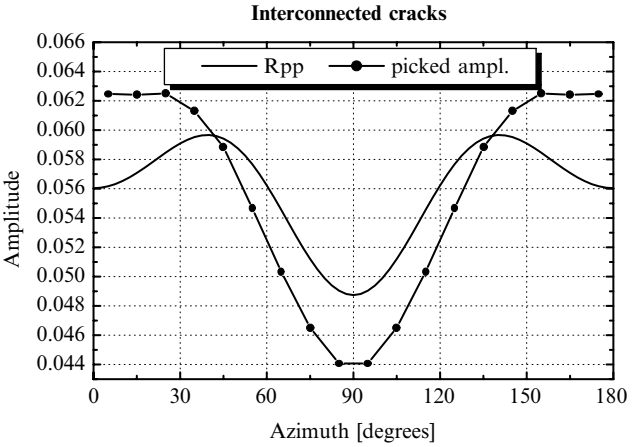

Figure 11 Synthetic data example, showing the effect of attenuation due to interconnected cracks on the amplitudes. The model contains gas-filled cracks with an aspect ratio of 10^{-4}, a crack density of 0.1, and the permeability is 1 D. Points are amplitudes picked from the data and the solid line shows the reflection coefficient for comparison. The symmetry directions are still detectable, but the estimation of correct crack parameters will not be possible.

Equant porosity

The most important mechanism of attenuation due to fluid flow is diffusion from the cracks into equant pores in the surrounding matrix. To include this effect in the calculation of the elastic constants, the expression for K in (3) has to be changed to (Pointer *et al.* 2000)

$$K = \left\{\frac{a}{\pi c}\frac{\kappa_f}{\mu}\left(\frac{\lambda+2\mu}{\lambda+\mu}\right)\right\}\left\{1+\frac{3(1-i)J}{2c}\right\}^{-1}, \qquad (9)$$

where

$$J^2 = \Phi_m \kappa_f K_m / 2\omega\eta_f.$$

Φ_m and K_m are the matrix porosity and permeability of the rock without any cracks. In this case, there are three variables influencing attenuation that will be of interest: porosity, permeability and fluid viscosity.

Figures 12 and 13 show plots of the imaginary part of U_{11} as a function of the product of porosity and permeability for brine- and oil-filled cracks at different aspect ratios. In the case of brine fill, the maximum attenuation will occur at relatively low porosity and permeability values. This maximum is moved to higher porosities and permeabilities if the

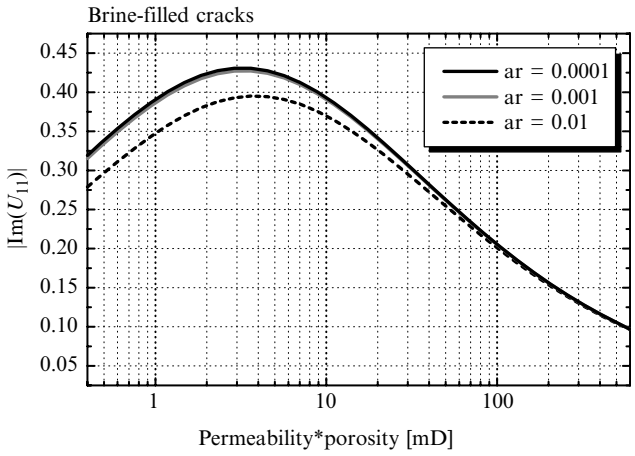

Figure 12 Equant porosity; dependence of the imaginary part of U_{11} on *permeability*porosity* for different aspect ratios. Cracks are brine-filled (see Table 3 for fluid properties). Maximum values lie at the lower end of the *permeability*porosity* scale.

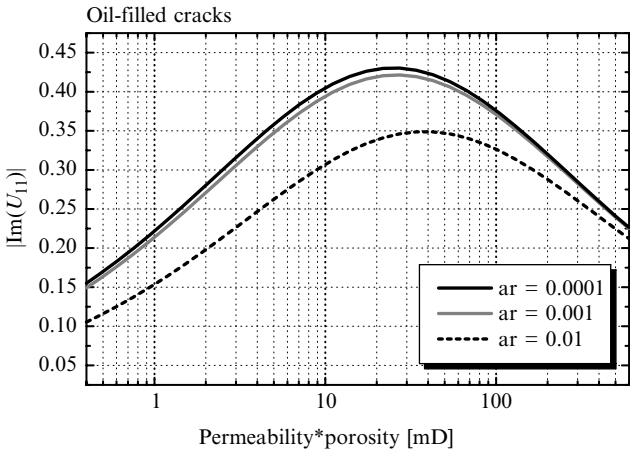

Figure 13 As Fig. 12 for oil-filled cracks (increased viscosity, see Table 3). The maximum is moved to higher permeability and porosity values.

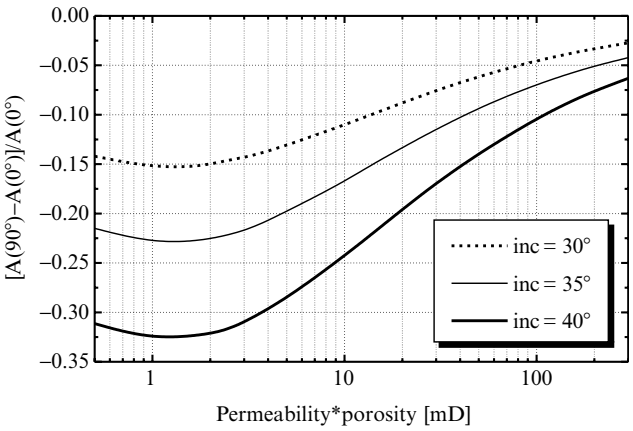

Figure 14 Relative change in amplitudes between the fracture strike and the fracture normal due to attenuation for equant porosity. Dependence on *permeability*porosity*. Cracks are brine-filled with an aspect ratio of 0.001 and a crack density of 0.1. Values are evaluated at incident phase angles of 30°, 35° and 40°. They exceed 10% for almost the entire range of permeability and porosity values.

cracks are oil-filled, i.e. the fluid viscosity is increased. In contrast to the case of interconnected cracks, fluid flow here occurs on a local scale. Thus little energy is dissipated by fluids moving from cracks into the surrounding pore space if the porosity and permeability are high. In the upper limit the cracks will essentially be drained, i.e. they approach the state of empty cracks. If, on the other hand, porosity and/or permeability tend to zero, the model describes isolated fluid-filled cracks. In general the curves in Figs 12 and 13 demonstrate that attenuation due to equant porosity will be effective over a wide parameter range. Many combinations of porosity and permeability values yield a product that falls into the range of the maxima seen in the plots.

As in the case of interconnected cracks, the relative change in attenuated amplitudes was computed for a defined model space. The same background model was used (Table 1), the cracks were brine-filled with an aspect ratio of 0.001, a half-thickness of 0.1 mm and a crack density of 0.1. The quantity *permeability*porosity* varied between 0.5 and 300 mD. Figure 14 shows a plot of the resulting amplitude change at angles of incidence of 30°, 35° and 40° as a function of *permeability*porosity*. For the highest angle of incidence, the values exceed 15% over a range from 0.5 to 40 mD and the maximum values lie around 32%. Even at angles of incidence of 30° and 35°, the relative amplitude change due to attenuation exceeds 10% for a large part of the parameter range. These numbers are clearly of the same order of magnitude as the azimuthal variation in reflection coefficients. Numerous parameter combinations would give values of *permeability*porosity* that fall into the above range, where

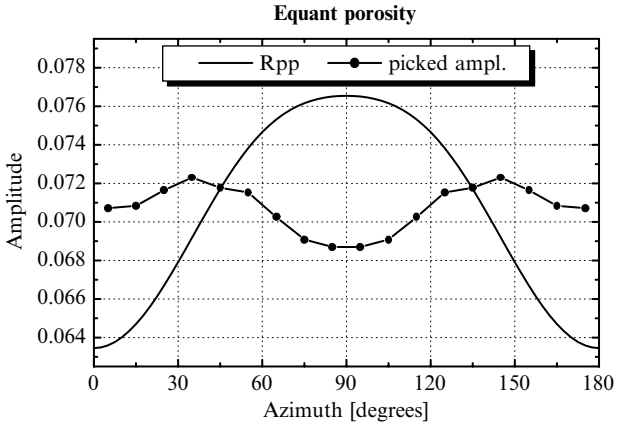

Figure 15 Synthetic data example from Fig. 6 with attenuation due to equant porosity in the fractured layer. The porosity is 10% and the permeability 50 mD. The azimuthal amplitude variation that the reflectivity produces (solid line) is cancelled in the data (points) by attenuation. Even the symmetry orientations will not be detectable.

attenuation is significant. Since the maxima in Fig. 13 will occur farther to the right for higher fluid viscosities, we can state that for any permeability and porosity commonly found in rocks, anisotropic attenuation due to equant porosity in a fractured overburden is an issue that can influence the amplitudes as much as the reflectivity.

A synthetic data example is plotted in Fig. 15. The model corresponds to that used for Fig. 6, but now attenuation is introduced in the fractured layer. The permeability is 50 mD

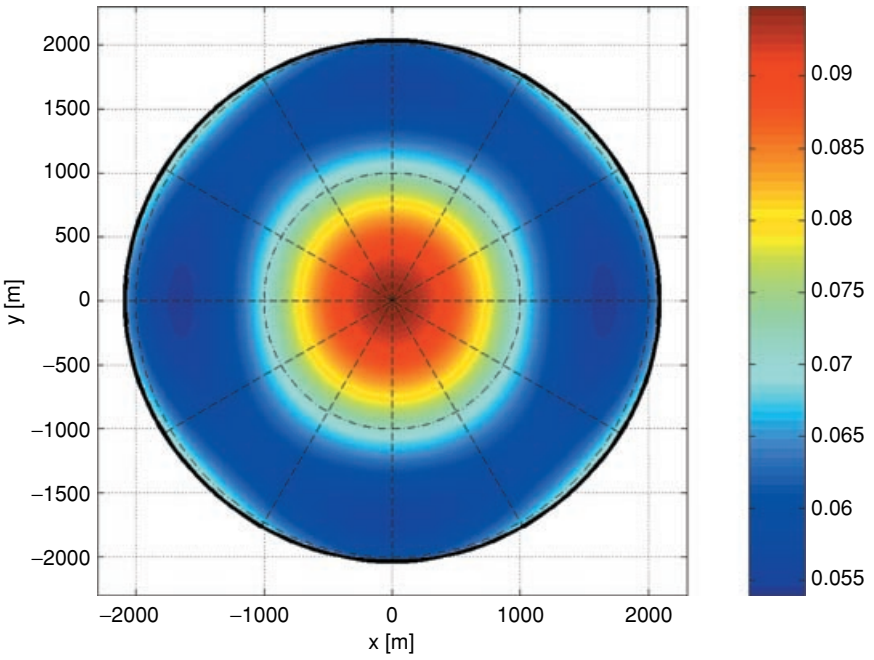

Figure 16 Reflected and attenuated amplitudes for the model used in Figs 1, 6 and 15. The two effects cancel each other out at all offsets, so that the resulting amplitude signature does not vary with azimuth. The amplitudes give no indication of fracturing in the target, unless the effect of attenuation is removed.

and the porosity 10%. Here the attenuation effect more or less cancels out the azimuthal amplitude variation that is produced by the reflectivity. This is fatal for the amplitude analysis, since even the symmetry directions will no longer be detectable and the data give no indication of fracturing in the target layer.

In order to give an overall picture of the effect, the function of the reflection coefficient combined with attenuation is plotted over the entire range of offsets in Fig. 16. The resulting amplitude signature is nearly isotropic at all angles of incidence, so that the detection of fractures will not be possible at any offset.

A second data example was generated for a model with two fractured layers that differ in their fracture orientation. Attenuation was introduced in the top HTI layer, whilst the reflection from the base of the lower cracked layer served as the target. Detailed model parameters are given in Table 4. In Fig. 17, the amplitudes picked from the data at an angle of incidence of 41° are plotted against azimuth together with the reflection coefficient. This example demonstrates how attenuation in the overburden can completely alter the signature of reflected amplitudes and thus make their use for fracture characterization impossible. The data give no indication of the symmetry inherent in the reflection coefficient at the target horizon. Moreover, the amplitudes would even predict a symmetry direction that conforms neither with the fracture set in the upper HTI layer nor with the one in the lower medium. This is demonstrated by the $\cos[2(\Phi-\Phi_0)]$ function (Φ denotes azimuth), which is fitted to the data and shown as the grey solid line on the plot. It is vital to remove the effect of attenuation in the overburden prior to the amplitude analysis to be able to gain some information about fractures in the target layer.

Table 4 Properties of the background media and crack parameters corresponding to the model with two fractured layers

Layer	v_P (m/s)	v_S (m/s)	Density (kg/m^3)	Thickness (m)
(1) Isotropic	3400	1700	2400	700
(2) HTI (120°)	3600	1980	2450	300
(3) HTI (0°)	4000	2400	2550	300
(4) Isotropic	4600	2760	2700	Half-space

Layer	Aspect ratio	Crack density	Crack infill	Porosity (%)	Permeability (mD)
(2) HTI (120°)	0.001	0.1	Brine	10	50
(3) HTI (0°)	0.001	0.05	Brine	0	0

CONCLUSIONS

Anisotropy in the overburden has to be considered as a realistic issue in many seismic data sets. We have shown that it strongly affects the variation of amplitudes with azimuth, which is used to characterize fracture systems in the

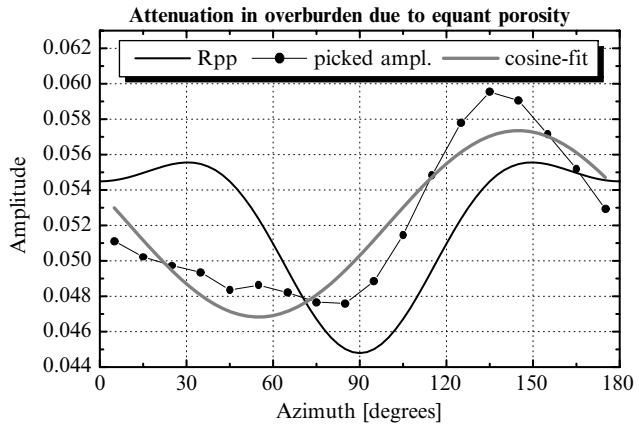

Figure 17 Attenuation in a fractured overburden with a fracture strike different from that of the target layer (see Table 4 for the model parameters). The signature of the reflection coefficient (black solid line) is altered completely. The amplitude data (dots), picked at an angle of incidence of 41°, suggest incorrect orientations of the symmetry planes shown by the grey solid line.

target layer. It is vital to include anisotropic overburden effects in the amplitude analysis in order to gain correct results. Regarding the measured amplitudes only as a representation of the plane-wave reflection coefficient at the target will lead to major errors. In this study, we have demonstrated over which parameter ranges transmission coefficients, geometric spreading and attenuation influence the amplitude signature considerably.

The transmission coefficients can generally be ignored. They yield azimuthal amplitude changes that are far lower than those of the reflection coefficients and they will not be detectable in a real data case.

The divergence effect can cause significant variations in amplitudes with azimuth, depending on crack parameters, the background v_S/v_P-ratio and the layer thickness. Since the NMO velocities cannot be used to define spreading factors in anisotropic media, another way has to be found to correct for the geometric spreading, if it is an issue for the amplitude analysis. In cases where its azimuthal variation can be neglected, the velocity function of the fracture strike should be used for an isotropic geometric spreading correction. It should be noted that the results obtained here for a single fractured layer cannot be extrapolated to the case of multiple fractured layers, since the effect is not additive.

The most important issue is attenuation due to equant porosity and interconnected cracks, which is effective over a very wide parameter range. It yields changes in amplitudes with azimuth that are comparable to the azimuthal variation of the reflection coefficient. Attenuation will make a correct amplitude analysis impossible, especially when the fractures in the overburden are orientated differently from those in the target layer. On the other hand, it is desirable to use the information that is contained in the azimuthal variation of transmitted amplitudes to define fractures in the overburden. This may be possible if the effects of attenuation and reflection coefficients can be separated by a layer-stripping technique.

There is not yet any experimental data that could satisfactorily verify the theories for the attenuation mechanisms used here (Hudson, Pointer and Liu 2001), and other theories have also been proposed (e.g. Thomsen 1995). The model assumed in Hudson's theory contains perfectly aligned microcracks of the same size. A more realistic representation of the rock should consider a distribution of crack orientations (Tod 2001) and cracks or fractures at different scales. Nevertheless, the results of this study give an idea of the possible influence of anisotropic overburden effects and attenuation in particular on seismic amplitudes. They provide a reasonable explanation of why the results of amplitude analysis often do not agree with the results of velocity analysis. With more accurate descriptions of the rock physics, the pore-space geometry and the processes of fluid exchange, there may be scope for using these effects as additional attributes to characterize fractured reservoirs.

ACKNOWLEDGEMENTS

S.M. thanks Mark Chapman and Enru Liu at the Edinburgh Anisotropy Project as well as Iain Bush, Dave Hill and Geoffrey King at WesternGeco for helpful comments and discussions. Suggestions from two anonymous reviewers very much helped to improve the manuscript. This study was sponsored by and performed at WesternGeco, UK. S.M. is currently supported by the sponsors of the Edinburgh Anisotropy Project (EAP) and the work is published with the approval of the Executive Director of the British Geological Survey (NERC).

REFERENCES

Gray D. and Head K. 2000. Fracture detection in Manderson Field: a 3-D AVAZ case history. *The Leading Edge* **19**, 1214–1221.

Horne S.A. and MacBeth C. 1997. AVA observations in walkaround VSPs. 67th SEG Meeting, Dallas, USA, Expanded Abstracts, 290–293.

Horne S.A., McGarrity J.P., Sayers C.M., Smith R.L. and Wijnands F. 1998. Fractured reservoir characterization using multi-azimuthal walkaway VSPs. 68th SEG Meeting, New Orleans, USA, Expanded Abstracts, 1640–1643.

Hsu C.-J. and Schoenberg M. 1993. Elastic waves through a simulated fractured medium. *Geophysics* **58**, 964–977.

Hudson J.A. 1981. Wave speeds and attenuation of elastic waves in material containing cracks. *Geophysical Journal of the Royal Astronomical Society* **64**, 133–150.

Hudson J.A. 1986. A higher order approximation to the wave propagation constants for a cracked solid. *Geophysical Journal of the Royal Astronomical Society* **87**, 265–274.

Hudson J.A., Liu E. and Crampin S. 1996. The mechanical properties of materials with interconnected cracks and pores. *Geophysical Journal International* **124**, 105–112.

Hudson J.A., Pointer T. and Liu E. 2001. Effective medium theories for fluid-saturated materials with aligned cracks. *Geophysical Prospecting* **49**, 509–522.

Kühnel T. 1998. *The influence of structure on seismic parameter estimation in anisotropic media*. PhD thesis, University of Edinburgh.

Liu E., Hudson J.A. and Pointer T. 2000. Equivalent medium representation of fractured rock. *Journal of Geophysical Research* **105** (B2), 2981–3000.

Lynn H.B., Beckham W.E., Simon K.M., Bates C.R., Layman M. and Jones M. 1999. P-wave and S-wave azimuthal anisotropy at a naturally fractured gas reservoir, Bluebell-Altamont field, Utah. *Geophysics* **64**, 1312–1328.

MacBeth C. 1999. Azimuthal variation in P-wave signatures due to fluid flow. *Geophysics* **64**, 1181–1192.

MacBeth C., Jakubowitz H., Kirk W., Li X.-Y. and Ohlsen F. 1997. Fracture-related amplitude variations with offset and azimuth in marine seismic data. 59th EAGE Conference, Geneva, Switzerland, Extended Abstracts, B054.

Mallick S., Chambers R.E. and Gonzalez A. 1996. *Method for Determining the Principal Axes of Azimuthal Anisotropy from Seismic P-wave Data*. US Patent No. 5508973.

Mallick S., Craft K.L., Meister L.J. and Chambers R.E. 1998. Determination of the principal directions of azimuthal anisotropy from P-wave seismic data. *Geophysics* **63**, 692–706.

Newman P. 1973. Divergence effects in a layered earth. *Geophysics* **38**, 481–488.

Pérez M.A., Gibson R.L. and Toksöz M.N. 1999. Detection of fracture orientation using azimuthal variation of P-wave AVO responses. *Geophysics* **64**, 1253–1265.

Pointer T., Liu E. and Hudson J.A. 2000. Seismic wave propagation in cracked porous media. *Geophysical Journal International* **142**, 199–231.

Rüger A. 1996. *Reflection coefficients and azimuthal AVO analysis in anisotropic media*. PhD thesis, Colorado School of Mines.

Rüger A. and Tsvankin I. 1997. Using AVO for fracture detection: analytic basis and practical solutions. *The Leading Edge* **16**, 1429–1434.

Schoenberg M. 1983. Reflection of elastic waves from periodically stratified media with interfacial slip. *Geophysical Prospecting* **31**, 265–292.

Schoenberg M. and Douma J. 1988. Elastic wave propagation in media with parallel fractures and aligned cracks. *Geophysical Prospecting* **36**, 571–590.

Thomsen L. 1995. Elastic anisotropy due to aligned cracks in porous rock. *Geophysical Prospecting* **43**, 805–829.

Tod S.R. 2001. The effects on seismic waves of interconnected nearly aligned cracks. *Geophysical Journal International* **146**, 249–263.